

Formation of GW230529 from Isolated Binary Evolution and Its Electromagnetic Counterparts

JIN-PING ZHU ^{1,2,*} RUI-CHONG HU ^{3,4,*} YACHENG KANG ^{5,6} BING ZHANG ^{3,4} HUI TONG ^{1,2} LIJING SHAO ^{6,7}
AND YING QIN ⁸¹*School of Physics and Astronomy, Monash University, Clayton Victoria 3800, Australia*²*OzGrav: The ARC Centre of Excellence for Gravitational Wave Discovery, Australia*³*Nevada Center for Astrophysics, University of Nevada, Las Vegas, NV 89154, USA*⁴*Department of Physics and Astronomy, University of Nevada, Las Vegas, NV 89154, USA*⁵*Department of Astronomy, School of Physics, Peking University, Beijing 100871, China*⁶*Kavli Institute for Astronomy and Astrophysics, Peking University, Beijing 100871, China*⁷*National Astronomical Observatories, Chinese Academy of Sciences, Beijing 100012, China*⁸*Department of Physics, Anhui Normal University, Wuhu, Anhui 241002, China*

ABSTRACT

In this *Letter*, we explore the formation of the mass-gap black hole-neutron star (mgBHNS) merger detected in gravitational wave (GW) event, i.e., GW230529, from the isolated binary evolution channel, and study potential signatures of its electromagnetic counterparts. By adopting the ‘delayed’ supernova prescription and reasonable model realizations, our population synthesis simulation results can simultaneously match the rate densities of mgBHNS and total BHNS mergers inferred from the population analyses, along with the population distribution of the BH mass in BHNS mergers reported by the LIGO-Virgo-KAGRA Collaboration. Because GW230529 contributes significantly to the inferred mgBHNS rate densities, we suggest that GW230529 can be explained through the isolated binary evolution channel. Considering the AP4 (DD2) equation of state, the probability that GW230529 can make tidal disruption is 12.8% (63.2%). If GW230529 is a disrupted event, its kilonova peak apparent magnitude is predicted $\sim 23 - 24$ mag, and hence, can be detected by the present survey projects and LSST. Since GW230529 could be an off-axis event inferred from the GW observation, its associated gamma-ray burst (GRB) might be too dim to be observed by γ -ray detectors, interpreting the lack of GRB observations. Our study suggests the existence of mgBHNS mergers formed through the isolated binary evolution channel due to the discovery of GW230529, indicating that BHNS mergers are still likely to be multimessenger sources that emit GWs, GRBs, and kilonovae. Although mgBHNS mergers account for $\sim 50\%$ cosmological BHNS population, we find that $\gtrsim 90\%$ disrupted BHNS mergers are expected to originate from mgBHNS mergers.

Keywords: Gravitational waves (678); Neutron stars (1108); Black holes (162)

1. INTRODUCTION

Black hole–neutron star (BHNS) mergers are prime search targets for the ground-based gravitational-wave (GW) detectors, including LIGO (LIGO Scientific Collaboration et al. 2015), Virgo (Acernese et al. 2015), and KAGRA (Aso et al. 2013). Until the end of the GW third observing run (O3), the first two BHNS mergers

were identified by the LIGO-Virgo-KAGRA (LVK) Collaboration (Abbott et al. 2021a), with GW200105 being a merger between a $8.9^{+1.2}_{-1.5} M_{\odot}$ BH and a $1.9^{+0.3}_{-0.2} M_{\odot}$ NS, and GW200115 being a merger between a $5.7^{+1.8}_{-2.1} M_{\odot}$ BH and a $1.5^{+0.7}_{-0.3} M_{\odot}$ NS (all measurements quoted at the 90% credible level). During O3, the LVK Collaboration reported three additional marginal BHNS candidates (Abbott et al. 2021b; The LIGO Scientific Collaboration et al. 2021; Abbott et al. 2023), with GW190426_152155 involving a $5.7^{+3.9}_{-2.3} M_{\odot}$ BH and a $1.5^{+0.8}_{-0.5} M_{\odot}$ NS, GW190917_114630 involving a $9.7^{+3.4}_{-3.9} M_{\odot}$ BH and a $2.1^{+1.1}_{-0.4} M_{\odot}$ NS, as well as GW191219_163120 involving a $31.1^{+2.2}_{-2.8} M_{\odot}$ BH and a $1.17^{+0.07}_{-0.06} M_{\odot}$ NS. GWTC-3

Corresponding author: Jin-Ping Zhu, Rui-Chong Hu, Bing Zhang
jin-ping.zhu@monash.edu, ruichong.hu@unlv.edu,
bing.zhang@unlv.edu

* These authors contributed equally to this work

also includes a puzzling GW event, GW190814, composed of a $22.2 - 24.3 M_{\odot}$ primary BH and a $2.50 - 2.67 M_{\odot}$ secondary compact object with unclear origin (Abbott et al. 2020). The LVK Collaboration also discovered a similar, but marginal GW candidate, namely GW200210.092254 (Abbott et al. 2023), with component masses inferred to be $24.1^{+7.5}_{-4.6} M_{\odot}$ and $2.83^{+0.47}_{-0.42} M_{\odot}$, respectively.

The X-ray and radio observations of Galactic pulsars implied a likely NS maximum mass of $\sim 2 - 2.3 M_{\odot}$ (e.g., Antoniadis et al. 2013; Alsing et al. 2018; Romani et al. 2022) while Galactic BHs in X-ray binaries were inferred to have a lower boundary close to $\sim 5 M_{\odot}$ (Bailyn et al. 1998; Özel et al. 2010; Farr et al. 2011), leading to the conjecture of the presence of a mass gap between the heaviest NSs and lightest BHs. However, recent electromagnetic (EM) observations of non-interacting binary systems (Thompson et al. 2019; Rivinius et al. 2020; Andrews et al. 2022) and gravitational microlensing events (Wyrzykowski & Mandel 2020) indicated that the mass gap might be partially polluted. The population properties of O3 BHNS candidates suggested a relative dearth of events with masses in the mass gap (Zhu et al. 2022b; Ye & Fishbach 2022; Biscoveanu et al. 2023), which was also supported by the population study on merging compact binaries in GWTC-3 (Abbott et al. 2023). Whether there is a mass gap or not can shed light on supernova (SN) mechanisms for the formation of NSs and BHs, with the rapid model giving rise to the mass gap, while the delayed model does not (Fryer et al. 2012). Population synthesis simulations revealed that BHs in $\sim 30 - 80\%$ BHNS mergers can have a mass in the mass gap by considering the delayed SN model (Shao & Li 2021; Drozd et al. 2022). It is expected that future detection of merging mass-gap BHNS (mgBHNS) binaries through GW observations can give a better constraint on the SN mechanisms.

Binary NSs (BNSs) and BHNSs have long been proposed to be progenitors of some fast-evolving EM transients, including gamma-ray bursts (GRBs; Paczynski 1986, 1991; Eichler et al. 1989; Narayan et al. 1992; Zhang 2018; Gottlieb et al. 2023) and kilonovae (Li & Paczyński 1998; Metzger et al. 2010). While BNS mergers were confirmed as the origin of GRBs and kilonovae thanks to the associations between GW170817 (Abbott et al. 2017a), GRB170817A (Abbott et al. 2017b; Goldstein et al. 2017; Savchenko et al. 2017; Zhang et al. 2018), and AT2017gfo (e.g., Abbott et al. 2017c; Arcavi et al. 2017; Coulter et al. 2017; Drout et al. 2017; Evans et al. 2017; Kasen et al. 2017; Kasliwal et al. 2017; Kilpatrick et al. 2017; Pian et al. 2017; Smartt et al. 2017), the joint observations of the O3 BHNS GW

candidates and their associated EM counterparts, especially for kilonova emissions, were absent. One possible reason for the lack of kilonova detection following O3 BHNS GW signals could be the challenge of rapidly achieving full distance and volumetric coverage for the probability maps of the LVK Collaboration within the short kilonova duration by current survey projects (e.g., Coughlin et al. 2020; Kasliwal et al. 2020; Gompertz et al. 2020; Anand et al. 2021). Unlike BNS mergers, which typically eject a certain amount of materials to produce EM counterparts, the NS components in some merging BHNS binaries may directly plunge into their BH companions without generating any observable EM signals. NS tidal disruption tends to occur if the BHNS binaries have a low-mass BH with a high orbital aligned spin and a low-mass NS with a stiff EoS (Shibata & Taniguchi 2011; Foucart 2012; Kyutoku et al. 2013, 2015; Kawaguchi et al. 2016; Foucart et al. 2018; Zhu et al. 2020, 2021b; Hayashi et al. 2021; Sarin et al. 2022). More specifically, since primary BHs (produced from initially more massive star) formed through the classical CE scenario typically possess near-zero aligned spins (Qin et al. 2018; Fuller et al. 2019; Belczynski et al. 2020), tidal disruptions of most cosmological BHNS mergers are expected to occur if the BHs have a mass of $\lesssim 6 - 7 M_{\odot}$ and the NSs have a mass of $\lesssim 1.5 M_{\odot}$ (e.g., Zhu et al. 2021a, 2022b). If the mass gap does exist, the mass space that allows NS tidal disruption and produces bright EM signals could be limited. Because O3 BHNS candidates have BH masses of $\gtrsim 5 M_{\odot}$ inferred from GW observations, their posterior mass distributions mostly lie outside the tidal disruption mass range (Abbott et al. 2021a; Zhu et al. 2021a, 2022b; D’Orazio et al. 2022). Thus, it is likely that the EM counterparts associated with these BHNS candidates were intrinsically missing. Additionally, although a few O3 BHNS candidates still have low probabilities of undergoing tidal disruption and producing kilonova emissions, the brightness of these kilonovae might be too dim to be detected by current survey telescopes due to their remote distance from us (Zhu et al. 2021a).

The discovery of mgBHNS mergers through GW observations can provide an opportunity to constrain SN mechanisms and isolated formation channel of compact binaries. Furthermore, mgBHNS mergers are more likely to have tidal disruption and produce observable EM counterparts. Multimessenger observations of BHNS mergers between GWs and EMs can be more easily achieved if mgBHNS mergers exist. Most recently, the LVK Collaboration reported the first mgBHNS merger, GW230529, detected in the first part of the fourth observing run (The LIGO Scientific Col-

laboration et al. 2024). By adopting the combined posterior results inferred by the low-spin prior of the secondary component (i.e., the posterior sample of `Combined_PHM_lowSecondarySpin`; The LIGO Scientific Collaboration et al. 2024), the primary BH mass of GW230529 is $M_{\text{BH}} = 3.6^{+0.7}_{-1.2} M_{\odot}$ nearly filling in the mass gap, while its secondary NS mass is $M_{\text{NS}} = 1.43^{+0.59}_{-0.19} M_{\odot}$. The effective inspiral-spin and effective precessing-spin of GW230529 are $\chi_{\text{eff}} = -0.10^{+0.10}_{-0.17}$ and $\chi_{\text{p}} = 0.40^{+0.37}_{-0.34}$, respectively. The source has a redshift of $z = 0.043^{+0.023}_{-0.021}$, corresponding to a luminosity distance of $D_{\text{L}} = 197^{+107}_{-96}$ Mpc. Based on the population properties of currently detected BHNS mergers using the NSBH-POP model reported by The LIGO Scientific Collaboration et al. (2024), we find the rate densities of mgBHNS mergers with a primary BH mass $\lesssim 5 M_{\odot}$ and total BHNS mergers to be $R_{\text{mgBHNS}} = 18^{+58}_{-16} \text{ Gpc}^{-3} \text{ yr}^{-1}$ and $R_{\text{BHNS}} = 40^{+77}_{-29} \text{ Gpc}^{-3} \text{ yr}^{-1}$, respectively. Without the inclusion of GW230529, these rate densities change to be $R_{\text{mgBHNS}} = 0^{+10}_{-0} \text{ Gpc}^{-3} \text{ yr}^{-1}$ and $R_{\text{BHNS}} = 18^{+41}_{-15} \text{ Gpc}^{-3} \text{ yr}^{-1}$. Thus, GW230529 significantly increases the inferred rate of mgBHNS mergers.

In this *Letter*, we explore the formation of GW230529 through the isolated binary evolution channel and study the properties of its associated EM counterparts. Hereafter, the combined posterior sample inferred by the default low-spin prior of the secondary component released by the LVK Collaboration is employed for our studies on individual GW sources, including GW200105, GW200115, and GW230529 (Abbott et al. 2021a; The LIGO Scientific Collaboration et al. 2024).

2. POPULATION SYNTHESIS OF BHNS MERGERS AND FORMATION OF GW230529

2.1. Method

In this section, we employ the rapid binary population synthesis code COMPAS (version 02.39.00; Stevenson et al. 2017; Vigna-Gómez et al. 2018; Neijssel et al. 2019; Team COMPAS: Riley, J. et al. 2022) to explore the formation of GW230529 through the isolated binary evolution channel. To determine compact object masses during core-collapse SNe (CCSNe) of stars, the ‘delayed’ SN prescription (Fryer et al. 2012) is adopted, which allows for the production of mass-gap BHs (see also the stochastic recipe developed by Mandel & Müller 2020). We generate and evolve binary systems according to the fiducial population synthesis model described in Table 1 of Broekgaarden et al. (2021), with the maximum NS mass changed to $M_{\text{NS,max}} = 2.2 M_{\odot}$. We refer readers to Table 4 in Appendix for further details on other initial

conditions, parameter settings, and simulation settings we used.

We explore the variations of different common-envelope (CE) efficiencies ($\alpha_{\text{CE}} = 1, 2, 5, 10$) and the velocity dispersion of CCSNe natal kicks ($\sigma_{\text{CCSN}} = 100, 265 \text{ km s}^{-1}$; Hobbs et al. 2005) in the formation of BHNS mergers. The naming convention of our population synthesis models follows the pattern $\alpha X \sigma Y$, where X and Y are the corresponding values of α_{CE} and σ_{CCSN} . Our population synthesis simulations include 8 models, each evolving 10^6 binaries across 10 metallicity bins, totaling 10^7 binaries. We select BHNS merger systems if the final primary mass $M_1 > M_{\text{NS,max}}$ and secondary mass $M_2 < M_{\text{NS,max}}$, while we identify mgBHNS merger systems by further requiring the final primary mass $M_{\text{NS,max}} < M_1 < 5 M_{\odot}$. Since χ_{eff} and χ_{p} of GW NSBH mergers were measured to potentially have low distributions, consistent with those of BHNS mergers originating from the isolated binary evolution (e.g., Zhu et al. 2022b), we do not consider spin parameters in our selection criteria. Using Equation (2) in Broekgaarden et al. (2021), the redshift-dependent BHNS rate densities are calculated based on the metallicity-specific star formation rate density model, which combines the Madau & Dickinson (2014) star formation rate density with the Panter et al. (2004) galaxy mass function and the Langer & Norman (2006) mass-metallicity relation. The local BHNS rate densities are obtained by considering simulated events within a redshift of 0.25.

2.2. Results

The simulated local event rate densities of mgBHNS and BHNS mergers are listed in Table 1 and are displayed in Figure 1. In Table 1, we also calculate the confidence intervals for our simulated population synthesis rate densities to fall within the posterior distribution of $\mathcal{R}_{\text{mgBHNS}}$ and $\mathcal{R}_{\text{BHNS}}$ obtained from the population analyses reported by the LVK Collaboration (The LIGO Scientific Collaboration et al. 2024). The event rate densities of our population synthesis simulations are all within the 90% credible intervals of observed $\mathcal{R}_{\text{mgBHNS}}$ and $\mathcal{R}_{\text{BHNS}}$. We find that the models with a higher SN kick indicate a better agreement with the LVK’s observations. Among these population synthesis models, the model of $\alpha 2 \sigma 265$ exhibits the best consistency with the GW observations.

We show the distribution of the BH mass and NS mass for the $\alpha 2 \sigma 265$ population model in Figure 2. The source-frame medians with the 90% credible intervals of the inferred posterior samples for GW200105, GW200115, and GW230529 are also displayed. One can find that the combined model predicts that the majority

Table 1. Merger Rate Density of Population Synthesis Simulation

Model	$\mathcal{R}_{\text{mgBHNS}}$ ($\text{Gpc}^{-3}\text{yr}^{-1}$)	$\mathcal{R}_{\text{BHNS}}$ ($\text{Gpc}^{-3}\text{yr}^{-1}$)	CI
$\alpha 1\sigma 100$	57	149	0.89
$\alpha 2\sigma 100$	93	154	0.84
$\alpha 5\sigma 100$	74	86	0.42
$\alpha 10\sigma 100$	58	67	0.47
$\alpha 1\sigma 265$	9	39	0.62
$\alpha 2\sigma 265$	17	37	0.16
$\alpha 5\sigma 265$	22	28	0.41
$\alpha 10\sigma 265$	16	25	0.30

NOTE—The columns are (1) the population synthesis model; (2) the simulated local merger rate density of mgBHNS events in $\text{Gpc}^{-3}\text{yr}^{-1}$; (3) the simulated local merger rate density of total BHNS mergers in $\text{Gpc}^{-3}\text{yr}^{-1}$; (4) the credible interval.

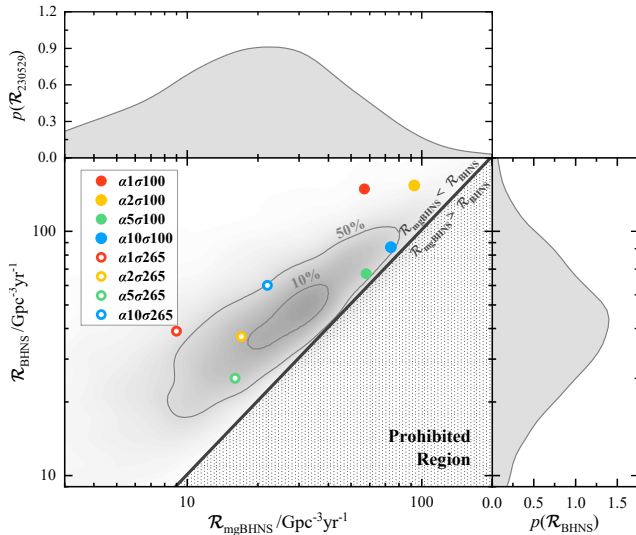


Figure 1. Simulated local rate density of mgBHNS and BHNS mergers. The red, orange, green, and blue points correspond to different envelope efficiencies of $\alpha_{\text{CE}} = 1, 2, 5, \text{ and } 10$, respectively. The solid and hollow points represent two NS natal kicks of $\sigma_{\text{NS}} = 100$ and 265 km s^{-1} . The top and right panels display the posteriors on the merger rate densities of mgBHNS and BHNS mergers obtained from [The LIGO Scientific Collaboration et al. \(2024\)](#). The 10% and 50% credible interval regions of the posteriors are marked as solid gray lines. The shadow region in the bottom right represents the prohibited parameter space where $\mathcal{R}_{\text{mgBHNS}} > \mathcal{R}_{\text{BHNS}}$.

of BHNS mergers can have a BH mass of $2.2 - 13.5 M_{\odot}$,

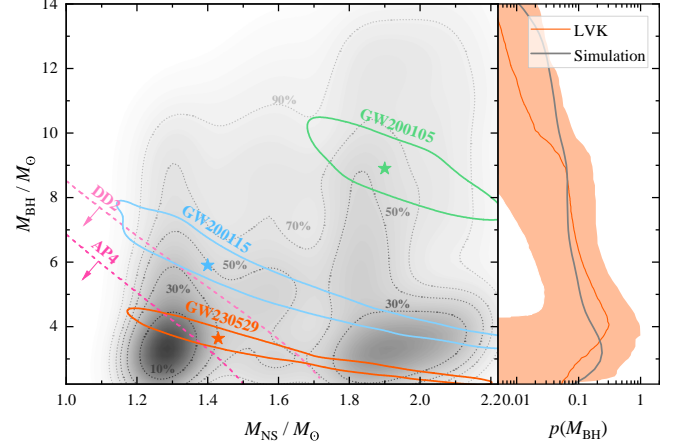


Figure 2. NS and BH masses of our population synthesis simulations. The grey dotted lines represent the credible interval regions of the simulation results, spanning from 10% to 90%, estimated using kernel density estimation. The source-frame medians (star points) along with their corresponding 90% credible intervals (solid lines) are illustrated for the posterior distributions of GW200105 (green), GW200115 (blue), and GW230529 (orange). The right panel shows the population distribution of the BH mass inferred by the GW observations ([The LIGO Scientific Collaboration et al. 2024](#)), contrasted with that derived from our population synthesis simulations (grey histogram). For an EoS of AP4 (DD2), non-spinning BHNS mergers with component masses located at the bottom left parameter space of the pink (light pink) dashed line can allow tidal disruption.

and a NS mass of $1.25 - 2.2 M_{\odot}$, with a concentration of $\sim 1.3 M_{\odot}$. The inferred properties of GW200105, GW200115, and GW230529 lie within the 70% credible interval of our simulated BHNS population. In particular, the medians with a large fraction of the posterior for the mgBHNS event, i.e., GW230529, recently reported by the LVK Collaboration significantly overlap with the highest probability region of the simulated BHNS population. We find that the predicted BH mass distribution is basically consistent with that of GW BHNS population inferred by the presently detected three high-confidence BHNS mergers. Compared with the current GW observations, where the BH mass peaks at $\sim 4 M_{\odot}$, our simulated BH population has a lower mass peak of $3.4 M_{\odot}$, which is approximately at the median of the posterior BH mass distribution of GW230529.

Overall, the posterior masses of GW230529 given by the LVK Collaboration are close to the highest probability region of the simulated BHNS population. Our population synthesis simulation results can simultaneously match the inferred event rate densities of mgBHNS and total BHNS mergers, along with the GW population distribution of the BH mass in BHNS mergers. Because GW230529 contributes significantly to the inferred

mgBHNS rate densities, one can expect that GW230529 can likely originate from the isolated binary evolution channel.

3. EM COUNTERPARTS OF GW230529 AND IMPLICATIONS FOR FUTURE BHNS EM OBSERVATIONS

GW230529 was only observed by LIGO Livingston and, hence, had a sky localization with a 90% credible area of $\sim 25600 \text{ deg}^2$ (The LIGO Scientific Collaboration et al. 2024), which was too wide for follow-up observations. There were no kilonova and GRB candidates reported after this event. In this section, we will study the tidal disruption probability and EM signals of GW230529. Furthermore, with the discovery of the existence of mgBHNS mergers, our previous understanding of the detectability of BHNS EM signals may change. We will also briefly explore the future detectability of BHNS EM signals based on our population synthesis simulations.

3.1. Tidal Disruption Probability

Whether tidal disruption can occur in a BHNS merger can be described by an empirical formula (Foucart et al. 2018)

$$\frac{M_{\text{total,fit}}}{M_{\text{NS}}^b} = \left[\max \left(\alpha \frac{1 - 2C_{\text{NS}}}{\eta^{1/3}} - \beta \tilde{R}_{\text{ISCO}} \frac{C_{\text{NS}}}{\eta} + \gamma, 0 \right) \right]^\delta, \quad (1)$$

which is used to calculate the total remnant mass outside the remnant BH horizon, where $\alpha = 0.406$, $\beta = 0.139$, $\gamma = 0.255$, $\delta = 1.761$, M_{NS}^b is the baryonic NS mass, $\eta = Q/(1+Q)^2$, $Q = M_{\text{BH}}/M_{\text{NS}}$ is the mass ratio between the BH mass M_{BH} and the NS mass M_{NS} , $C_{\text{NS}} = GM_{\text{NS}}/c^2 R_{\text{NS}}$ is the compactness dependent on the NS equation of state (EoS) with the gravitational constant G , speed of light c , and NS radius R_{NS} . The normalized inner stable circular orbit radius (Bardeen et al. 1972) can be expressed as $\tilde{R}_{\text{ISCO}} = 3 + Z_2 - \text{sign}(\chi_{\text{BH},z})\sqrt{(3 - Z_1)(3 + Z_1 + 2Z_2)}$, where $Z_1 = 1 + (1 - \chi_{\text{BH},z}^2)^{1/3}[(1 + \chi_{\text{BH},z})^{1/3} + (1 - \chi_{\text{BH},z})^{1/3}]$, $Z_2 = \sqrt{3\chi_{\text{BH},z}^2 + Z_1^2}$, and $\chi_{\text{BH},z}$ is the dimensionless spin parameter projected onto the orientation of orbital angular momentum, abbreviated as the BH aligned-spin hereafter. This formula can be more accurately applied in the range of $Q \in [1, 7]$, $\chi_{\text{BH}} \in [-0.5, 0.9]$, and $C_{\text{NS}} \in [0.13, 0.182]$ (Foucart et al. 2018). BHNS mergers with component masses located in the parameter space of $M_{\text{total}} > 0$ can undergo tidal disruption and generate EM signals.

We consider two specific EoSs commonly used in the literature, among which AP4 (Akmal & Pandharipande

1997) is one of the most probable EoSs with a Tolman-Oppenheimer-Volkoff mass of $M_{\text{TOV}} = 2.22 M_\odot$, while DD2 (Typel et al. 2010) is one of the stiffest EoSs constrained by GW170817 (Abbott et al. 2018a, 2019), with $M_{\text{TOV}} = 2.42 M_\odot$. We calculate the baryonic NS mass in Equation (1) as follow: $M_{\text{NS}}^b = M_{\text{NS},\odot} + A_1 \times M_{\text{NS},\odot}^2 + A_2 M_{\text{NS},\odot}^3$, where $M_{\text{NS},\odot} = M_{\text{NS}}/M_\odot$, and we adopt the fitting values $A_1 = 0.045$ (0.046) and $A_2 = 0.023$ (0.014) for an EoS of AP4 (DD2) from Gao et al. (2020). The NS compactness is given by the fitting formula from Coughlin et al. (2017), i.e., $C_{\text{NS}} = 1.1056 \times (M_{\text{NS}}^b/M_{\text{NS}} - 1)^{0.8277}$.

Figure 3 shows the parameter space where the NS can be tidally disrupted using Equation (1). For a given $\chi_{\text{BH},z}$, BHNS mergers composed of a low-mass BH component and a low-mass NS component are more easily to have tidal disruption. The mass space that allows NS tidal disruption expands significantly with increasing $\chi_{\text{BH},z}$ and the adoption of a stiffer EoS. We display the 90% credible posterior distributions and the medians of component masses, as well as the medians of BH aligned-spins $\chi_{\text{BH},z}$, for GW200105, GW200115, and GW230529 (Abbott et al. 2021a; The LIGO Scientific Collaboration et al. 2024) in Figure 3. Based on the GW observed samples reported by the LVK Collaboration (Abbott et al. 2021a; The LIGO Scientific Collaboration et al. 2024), the explicit results of the tidal disruption probabilities for these three BHNS mergers are listed in Table 2. It is obvious that GW200105 is unlikely to make tidal disruption to generate any EM counterparts, because its BH and NS components are massive with the mass distribution significantly outside the tidal disruption region. Although GW200115 has BH and NS masses much lighter than those of GW200105, tidal disruption can occur with only a very low probability of $P_{\text{tidal}} = 2.76\%$ under the EoS of DD2. Compared with GW200105 and GW200115 whose BH masses are $\gtrsim 5 M_\odot$, GW230529, as a mgBHNS merger, occupies a larger portion of its mass parameter space located within the disruption region, especially when considering a stiffer EoS. More specifically, the tidal disruption probabilities are 12.8% and 63.2% by adopting the EoS of AP4 and DD2, respectively. The former value is similar to that reported in The LIGO Scientific Collaboration et al. (2024), which was obtained by marginalizing over the EoS.

3.2. Kilonova Properties

Tidal disruption of a BHNS merger can directly generate unbound lanthanide-rich dynamical ejecta, while other unswallowed material can form a disk around the remnant BH. Based on Zhu et al. (2020), one can calculate the mass of the dynamical ejecta by $M_{\text{d}} =$

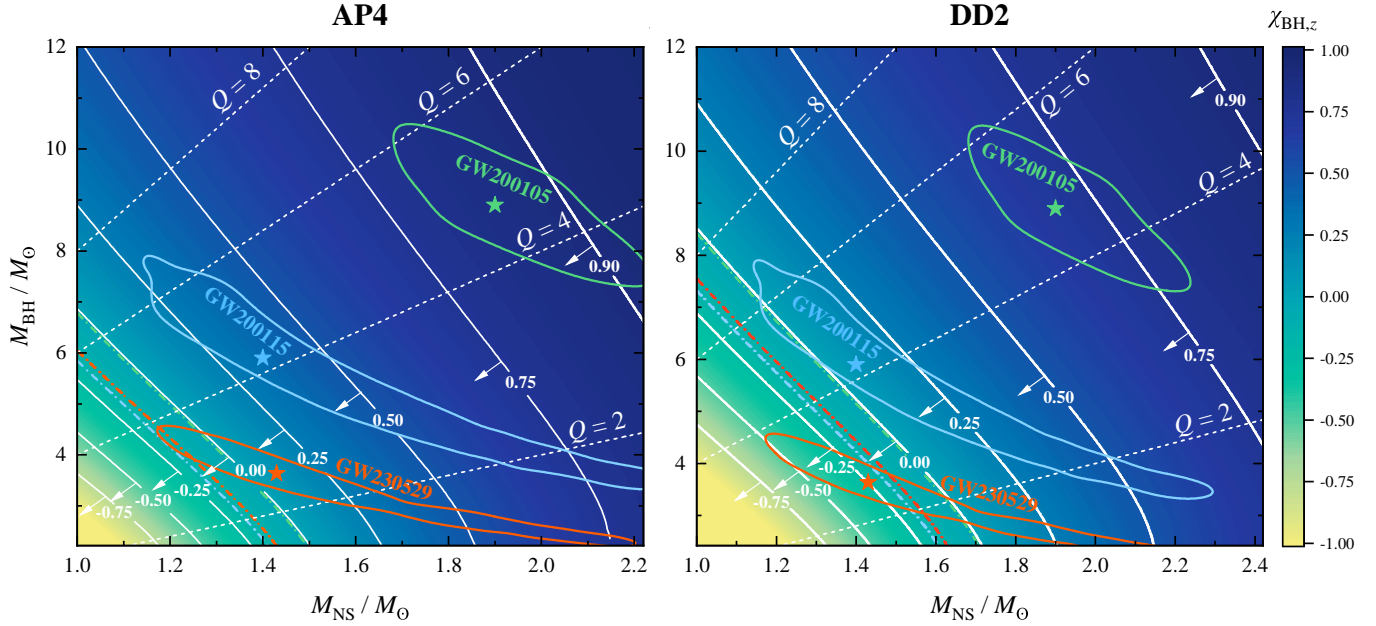


Figure 3. Source-frame mass parameter space for BHNS merger systems to allow NS tidal disruption. We mark the mass ratio from $Q = 2$ to 8 as dashed lines in each panel. The solid lines represent the primary BH aligned-spin $\chi_{\text{BH},z}$ from -0.75 to 0.90 . For a specific $\chi_{\text{BH},z}$, BHNS mergers with component masses located at the bottom left parameter space (denoted by the direction of the arrows) can undergo tidal disruption. For GW200105 (green), GW200115 (blue), and GW230529 (orange), the 90% credible posterior distributions (colored solid lines) and the medians (colored stars) are displayed, while the corresponding median values of $\chi_{\text{BH},z}$ for these three sources are marked as dashed-dotted lines.

Table 2. Tidal Disruption Probability, Kilonova Brightness, and GRB Detection Probability of BHNS Mergers

GW Event	EoS	P_{tidal}	m_g/mag	m_r/mag	P_{GRB}	
					$\theta_c = 3.5^\circ$	$\theta_c = 7^\circ$
GW200105	AP4	0%	—	—	—	—
	DD2	0%	—	—	—	—
GW200115	AP4	0%	—	—	—	—
	DD2	2.76%	$24.5^{+1.1}_{-1.3}$	$24.4^{+1.3}_{-1.1}$	0.004%	0.004%
GW230529	AP4	12.8%	$24.4^{+1.5}_{-1.9}$	$24.3^{+1.7}_{-1.9}$	0.35%	0.77%
	DD2	63.2%	$23.4^{+1.6}_{-1.3}$	$23.2^{+1.6}_{-1.4}$	1.56%	4.61%

NOTE—The columns are (1) the GW event; (2) the selected EoS; (3) the tidal disruption probability; (4) the median values with 90% credible intervals of g -band apparent magnitude distribution; (5) the median values with 90% credible intervals of r -band apparent magnitude distribution; (6) the GRB detection probability by considering the jet core opening angles of $\theta_c = 3.5^\circ$ and 7° .

$\min(f_{\text{max}}M_{\text{total,fit}}, M_{\text{d,fit}})$ and disk mass by $M_{\text{disk}} = M_{\text{tot,fit}} - M_{\text{d}}$, where f_{max} represents the maximum fraction of the dynamical ejecta mass in the total remnant mass as determined by the numerical relativity simulations (Kyutoku et al. 2015) and $M_{\text{d,fit}}$ can be obtained by substituting the fitting parameters in Equation (1) with $\alpha = 0.273$, $\beta = 0.035$, $\gamma = -0.153$ and $\delta = 1.491$. The root-mean-square velocity of the dynamical ejecta can be described by $v_{\text{rms,d}} = (-0.441Q^{-0.224} + 0.549)c$,

which is applied for $Q \in [1, 7]$. In addition to the tidal dynamical ejecta, the remnant disk can also produce lanthanide-free neutrino-driven wind ejecta caused by neutrino heating and intermediate-opacity viscosity-driven wind ejecta due to viscous heating and angular momentum transport. According to some numerical simulation results (e.g., Fernández et al. 2015; Just et al. 2015; Siegel & Metzger 2017), neutrino-driven ejecta and viscosity-driven ejecta can have masses of $\sim 1\%$

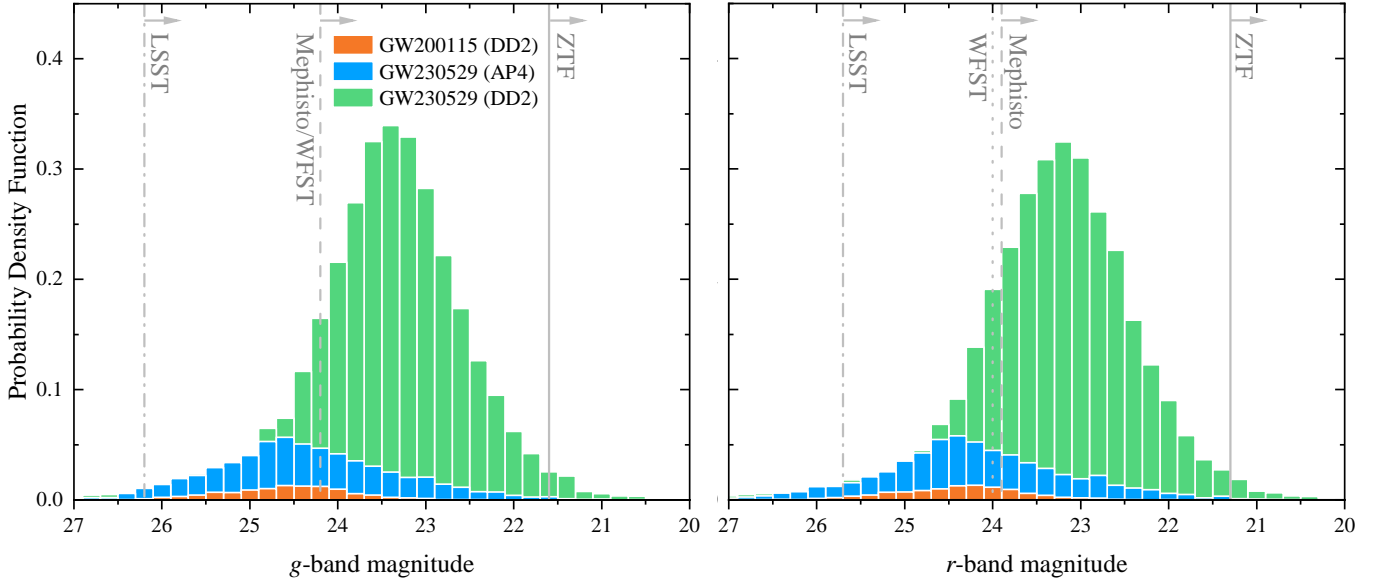


Figure 4. Probability density distributions of BHNS merger kilonova *g*-band (left panel) and *r*-band (right panel) peak magnitude for GW200115 and GW230529. The orange histograms represent the probability density for GW200115 with the consideration of the AP4 EoS, while the blue and green histograms show the probability densities for GW230529, employing the AP4 and DD2 EoSs, respectively. The gray solid, dashed, dotted, and dashed-dotted lines show the threshold depths of ZTF, Mephisto, WFST, and LSST for an exposure time of 300 s under the ideal observing conditions (Zhu et al. 2023). Here, the bin width of the histograms is set as $\Delta = 0.2$ mag.

and $\sim 20\%$ of the disk mass, respectively, with the root-mean-square velocities of $\sim 0.03c$ and $\sim 0.667c$. We set the gray opacities of neutrino-driven ejecta, and viscosity-driven ejecta as $1\text{ cm}^2\text{g}^{-1}$, $5\text{ cm}^2\text{g}^{-1}$, and $20\text{ cm}^2\text{g}^{-1}$ (Tanaka et al. 2020).

We use the detailed viewing-angle-dependent BHNS kilonova model presented by Zhu et al. (2020), which is essentially consistent with other models and simulations in the literature (e.g., Kawaguchi et al. 2016, 2020; Barbieri et al. 2019; Darbha et al. 2021; Zhu et al. 2022a; Gompertz et al. 2023), to simulate multi-band lightcurves of kilonova associated with BHNS GWs. The input parameters include binary parameters (M_{BH} , M_{NS} , and $\chi_{\text{BH},z}$) which can be obtained from the GW posterior results, EoS (i.e., AP4 and DD2), luminosity distance D_L , redshift z , and two viewing angle parameters (including the latitudinal viewing angle θ_{view} and the longitudinal viewing angle φ_{view}). Here θ_{view} equals the zenith angle between the total angular momentum and the line of sight θ_{JN} inferred from the observations of GW230529, while φ_{view} is randomly simulated between 0 and 2π .

In Figure 4, we show the probability density distributions of *g*- and *r*-band peak apparent magnitudes for the GW230529 kilonova. The medians with 90% credible intervals of the peak magnitude distributions are listed in Table 2. We also mark the threshold depths of four representative survey projects, including the Zwicky Transient Facility (ZTF; Bellm et al.

2019), the Multi-channel Photometric Survey Telescope (Mephisto¹), the Wide Field Survey Telescope (WFST; Wang et al. 2023) and the Large Synoptic Survey Telescope (LSST; LSST Science Collaboration et al. 2009), for an exposure time of 300 s in Figure 4. The peak apparent magnitudes of the GW230529 kilonova exhibit broad distributions with the medians of ~ 24.3 mag and ~ 23.3 mag when adopting the EoSs of AP4 and DD2, respectively. The medians of apparent magnitude distribution for DD2 are 1 mag brighter than those of GW200115, because GW230529 with $D_L = 197^{+107}_{-96}$ Mpc is much closer than GW200115 with $D_L = 310^{+150}_{-110}$ Mpc. Even though when considering a stiff EoS of DD2, we can find that ZTF could have a limited probability of observing the kilonova emission associated with GW230529. However, operational survey projects, including Mephisto and WFST, as well as future LSST can have enough detectability to discover the GW230529 kilonova if GW230529 can make tidal disruption.

3.3. GRB Properties

We adopt a single-Gaussian structured jet model (Zhang & Mészáros 2002) to describe the GRB angular distributions of the jet kinetic energy and Lorentz

¹ <http://www.mephisto.ynu.edu.cn>

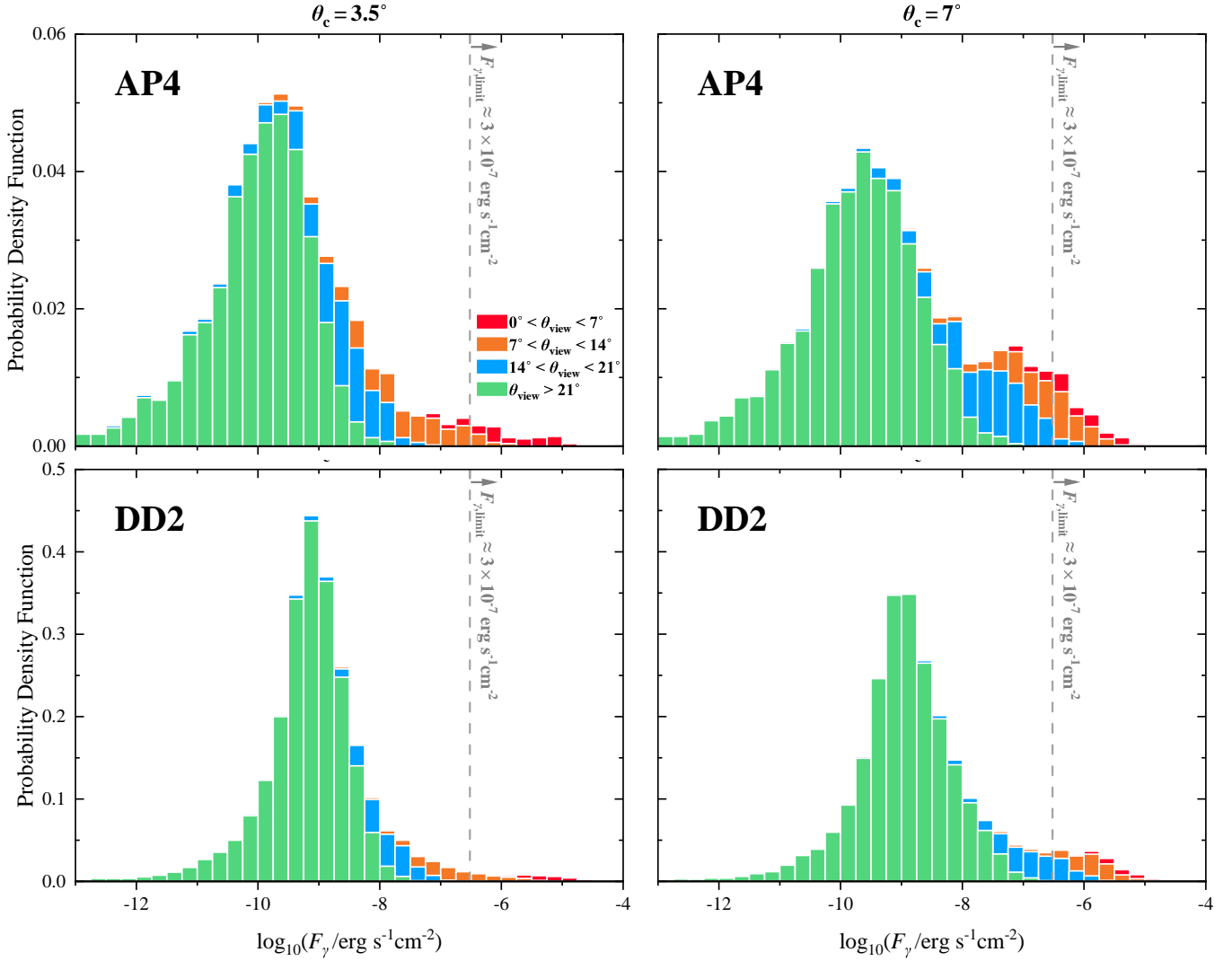


Figure 5. Probability density distributions of BHNS merger GRB γ -ray flux for GW230529. Two different core opening angles are considered: $\theta_c = 3.5^\circ$ (left panels) and 7° , as well as two EoSs, namely AP4 (top panels) and DD2 (bottom panels). The red, orange, blue, and green histograms represent GRB with latitudinal viewing angle ranges of $\theta_{\text{view}} < 7^\circ$, $7^\circ < \theta_{\text{view}} < 14^\circ$, $14^\circ < \theta_{\text{view}} < 21^\circ$, and $> 21^\circ$, respectively. The gray dashed lines indicate the effective sensitivity limit for γ -ray detectors. We note that the y -axis scalings differ between the top and bottom panels.

factor, i.e.,

$$\begin{aligned} \frac{dE}{d\Omega}(\theta) &= \varepsilon_c \exp\left(-\frac{\theta^2}{2\theta_c^2}\right), \\ \Gamma(\theta) &= \Gamma_c \exp\left(-\frac{\theta^2}{2\theta_c^2}\right) + 1, \end{aligned} \quad (2)$$

where Γ_c is the jet core Lorentz factor, θ_c is the jet core opening angle, $\varepsilon_c \approx E_{\text{K,jet}}/2\pi\theta_c^2$, and the kinetic energy of the Blandford–Znajek jet (Blandford & Znajek 1977) is $E_{\text{K,jet}} = \epsilon(1 - \xi)M_{\text{disk}}c^2\Omega_{\text{H}}^2 f(\Omega_{\text{H}})$ with $\epsilon \approx 0.015$ following Barbieri et al. (2019), the disk mass loss ratio $\xi \approx 0.2$ (Fernández et al. 2015; Just et al. 2015; Siegel & Metzger 2017), the dimensionless angular frequency at the BH horizon $\Omega_{\text{H}} = \chi_{\text{BH,f}}/2 \left(1 + \sqrt{1 - \chi_{\text{BH,f}}^2}\right)$, the

dimensionless spin of the final BH $\chi_{\text{BH,f}}$ calculated by using Equation (11) from Pannarale (2013), and the high-spin correction $f(\Omega_{\text{H}}) = 1 + 1.38\Omega_{\text{H}}^2 - 9.2\Omega_{\text{H}}^4$. The isotropic equivalent energy of the GRB prompt emission is given by (Salafia et al. 2015)

$$E_{\gamma,\text{iso}} = \eta_\gamma \int \frac{dE/d\Omega}{\Gamma^4(1 - \beta \cos \alpha)^3} d\Omega(\theta, \varphi), \quad (3)$$

where the radiation efficiency is typically adopted to $\eta_\gamma = 0.1$, $\beta = (1 - \Gamma^{-2})^{1/2}$, $\cos \alpha = \cos \theta \cos \theta_{\text{view}} + \sin \theta \sin \theta_{\text{view}} \cos \varphi$. Therefore, we can obtain the γ -ray flux by $F_\gamma = E_{\gamma,\text{iso}}/4\pi D_L^2 t_j$, where the jet duration is set to $t_j \approx 1$ s. Here, the GRB jet from BHNS mergers is assumed to be always launched towards the orbital angular momentum direction.

Based on the observations of both prompt and afterglow emissions from GW170817, we assume that the jet core Lorentz factor and opening angle are $\Gamma_c \sim 500$ and $\theta_c \sim 3.5^\circ$ (e.g., Lyman et al. 2018; Troja et al. 2020; Cao et al. 2023), respectively. Furthermore, because the amount of ejecta along the polar direction of BHNS mergers is typically much less than that of BNS mergers, the jets from BHNS mergers might not be effectively collimated. Therefore, we explore the variation of the jet core opening angle of $\theta_c = 7^\circ$, assessing its influence on the detection of GRBs associated with GW230529.

The viewing angle of GW230529 inferred by the LVK Collaboration is $\theta_{\text{view}} = 39_{-26}^{+33}$, suggesting that the associated GRB could be more likely an off-axis event. Based on this inferred viewing angle distribution, we model the γ -ray flux distributions of GRB associated with GW230529 by considering two EoSs in Figure 5. The GRBs with flux larger than the effective sensitivity limit in $1 - 10^4$ keV for Swift-BAT (Gehrels et al. 2004) and SVOM-ECLAIRS (Götz et al. 2014), i.e., $F_{\gamma, \text{limit}} \sim 3 \times 10^{-7} \text{ erg s}^{-1} \text{ cm}^{-2}$ (Song et al. 2019), are assumed to be triggered by GRB detectors. The detection probabilities of associated GRBs for GW200115 and GW230529 are listed in Table 2.

As shown in Figure 5, the flux distributions of GW230529-associated GRB are mostly much lower than the γ -ray sensitivity limit, peaking at $\sim 10^{-10} - 10^{-9} \text{ erg s}^{-1} \text{ cm}^{-2}$. If $\theta_c = 3.5^\circ$, GRB detection typically requires viewing angles of $\theta_{\text{view}} < 7 - 14^\circ$; if $\theta_c = 7^\circ$, the allowed viewing angles can be slightly larger with $\theta_{\text{view}} < 14 - 21^\circ$. When adopting an EoS of AP4, the probabilities of GRB detection could be always lower than 1%. By considering the stiffer EoS of DD2, more BHNS mergers can have tidal disruption, leading to a more massive disk and hence brighter GRBs. Nevertheless, since the GW observation suggested that GW230529 was likely to be an off-axis event, the detection of its associated GRB remains challenging. When adopting $\theta_c = 3.5^\circ$, the probability of GRB detection could be as low as 1.35%. Increasing θ_c to 7° can raise the detection probability to 4.61%. If GW230529 is a disrupted event, one may conclude that the absence of a detected GRB associated with GW230529 is likely due to it being an off-axis event, as indicated by the GW observation.

3.4. Implication of EM detectability for BHNS Mergers

In the standard binary evolution scenario, most BHs typically formed at wide orbits are expected to usually possess low spins (Qin et al. 2018; Fuller et al. 2019; Belczynski et al. 2020; Mandel & Smith 2021). BHs with high orbital aligned spin in BHNS mergers can originate

from tidal-induced spin-up (e.g., Qin et al. 2018; Bavera et al. 2020; Hu et al. 2022; Chattopadhyay et al. 2022) or accretion-induced spin-up (e.g., Wang et al. 2024; Xing et al. 2024; Zhu et al. 2024), which may only account for a small fraction of BHNS mergers. For simplicity, we assume that the spins of BHs in our simulated BHNS mergers are near-zero. Furthermore, we randomly generate $\sin \theta_{\text{view}}$ and φ_{view} within the ranges of $[0, 1]$ and $[0, 2\pi]$, respectively, for these simulated events. In Figure 2, we show the mass distribution of our population synthesis simulations introduced in Section 2.2, as well as the tidal disruption region for BHNS mergers with non-spinning BH components. One can see that BHNS mergers located in the highest probability region are always allowed to have tidal disruption. When considering the NS EoS of AP4, all BHNS mergers with BH mass higher than the mass gap are solely plunging events, whereas tidal disruption can only happen for mergers between an mgBH and a $\lesssim 1.4 M_\odot$ NS. For the stiffer EoS of DD2, a fraction of NSs with masses $\lesssim 1.4 M_\odot$ can be tidally disrupted by $5 - 8 M_\odot$ BHs. However, mgBHNS mergers would still be the dominant events causing disruption.

Based on our population synthesis simulation results, we then simulate the tidal disruption probability, kilonova detectable rate, and GRB detection rate for GW BHNS mergers detected in the near future GW observing era (e.g., O4b and O5). We conservatively consider BHNS mergers occurring within 300 Mpc, which is the observed distance of GW200105 and GW200115, as well as the representative distance of detectable BHNS mergers in O4 (Abbott et al. 2018b; Zhu et al. 2021b; Colombo et al. 2023; Gupta et al. 2023). We find that 100% and $\gtrsim 90\%$ disrupted BHNS mergers are expected to originate from mgBHNS mergers by adopting the EoS of AP4 and DD2, respectively. When the detection depth exceeds 24 mag, the survey projects can cover the majority of kilonovae associated with BHNS mergers. However, considering the rapid rise and decline of kilonovae, their signals may be challenging to be identified. Additionally, we find that the detection rate of GRBs originating from mgBHNS mergers is $\sim 0.1 - 0.4 \text{ yr}^{-1}$. Therefore, in the future, it may be possible to search for kilonova signals via the target-of-opportunity follow-up observations of both GW and GRB triggers, like the multimessenger observations between GW170817/GRB170817A/AT2017gfo.

4. CONCLUSION

In this *Letter*, we use COMPAS to explore the formation of GW230529, which is a mgBHNS merger between a $3.6_{-1.2}^{+0.7} M_\odot$ BH and a $1.43_{-0.19}^{+0.59} M_\odot$ NS reported

Table 3. EM Detectability of BHNS Mergers in 300 Mpc

EoS	Population	P_{tidal}	$R_{\text{tidal}}/\text{yr}^{-1}$	$R_{\text{kilonova}}/\text{yr}^{-1}$			$R_{\text{GRB}}/\text{yr}^{-1}$	
				22 mag	24 mag	26 mag	$\theta_c = 3.5^\circ$	$\theta_c = 7^\circ$
AP4	Mass-gap BHNS	17.1%	0.71	0.01	0.15	0.70	0.12	0.18
	High-mass BHNS	0	0	0	0	0	0	0
	Total BHNS	17.1%	0.71	0.01	0.15	0.70	0.12	0.18
DD2	Mass-gap BHNS	24.9%	1.04	0.06	0.79	1.03	0.20	0.33
	High-mass BHNS	3.4%	0.14	0.01	0.05	0.14	0.02	0.02
	Total BHNS	28.3%	1.18	0.27	0.07	1.17	0.20	0.35

NOTE—The columns are (1) the selected EoS; (2) the BHNS population, including mgBHNS mergers, high-mass BHNS mergers with BH mass of $\gtrsim 5 M_\odot$, and total BHNS mergers (3) the tidal disruption probability; (4) the tidal disruption rate in 300 Mpc; (5) the g -band kilonova detectable rate of BHNS mergers in 300 Mpc for three different detection depths of $m_g = 22, 24$, and 26 mag; (6) the detection rate of GRBs from BHNS mergers in 300 Mpc by considering two jet core opening angles of $\theta_c = 3.5^\circ$ and 7° .

by the LVK Collaboration. By adopting the ‘delayed’ SN prescription, our population synthesis simulations can simultaneously match the inferred event rate densities of the mgBHNS and total BHNS mergers obtained from the population analyses, along with the population distribution of the BH mass in BHNS mergers modeled by the LVK Collaboration. The mass posterior of GW230529 significantly overlaps with the highest probability region of the simulated BHNS population. Furthermore, mgBHNS mergers can also originate from dynamical formation in dense stellar environments or triple system, but the expected rate densities could be much lower than inferred GW mgBHNS rate densities (e.g., Fragione et al. 2020; Gupta et al. 2020; Ye et al. 2020; Tagawa et al. 2021). Since GW230529 contributes significantly to the current inferred mgBHNS rate densities, we suggest that GW230529 could originate from the isolated binary evolution channel.

By considering two specific EoSs of AP4 and DD2, the probabilities that GW230529 can have tidal disruption are 12.8% and 63.2%, respectively. If GW230529 is a disrupted event, the associated kilonova is predicted to have an apparent magnitude of $\sim 23 - 24$ mag, and hence, can be detected by the present survey projects and the LSST in the future. Since GW230529 could be an off-axis event inferred from the GW observation, its associated GRB might be too dim to be observed by γ -ray detectors, interpreting the lack of a detected GRB associated with the event. Our results are generally consistent with those suggested by other recent studies (e.g., Chandra et al. 2024; Ronchini et al. 2024).

The discovery of GW230529 revealed that the mass gap between $\sim 2.2 - 5 M_\odot$ may not exist. Previous studies indicated that most cosmological BHNS merg-

ers involving BH masses of $\gtrsim 5 M_\odot$ are usually hard to make tidal disruption and to generate bright EM signals (e.g., Zhu et al. 2021a,b, 2022b; Fragione 2021; Drozda et al. 2022). The existence of mgBHNS mergers suggests that BHNS mergers are still likely to be multimessenger sources that emit GWs, GRBs, and kilonovae. Although mgBHNS mergers account for $\sim 50\%$ of the cosmological BHNS population, we find that 100% and $\gtrsim 90\%$ disrupted BHNS mergers are expected to originate from mgBHNS mergers, when considering the EoSs of AP4 and DD2, respectively.

Software: COMPAS (version 02.39.00; Team COMPAS: Riley, J. et al. 2022); GWOSC, <https://gwosc.org>; Python, <https://www.python.org>; Matlab, <https://www.mathworks.com>; OriginPro, <https://www.originlab.com/originpro>

ACKNOWLEDGMENTS

Population Synthesis Simulations in this *Letter* made use of the COMPAS rapid binary population synthesis code (version 02.39.00), which is freely available at <http://github.com/TeamCOMPAS/COMPAS>. We thank the GWOSC (Gravitational Wave Open Science Center; <https://gwosc.org>) for making the data of GW230529 publicly available at <https://doi.org/10.7935/6k89-7q62>. We thank Floor Broekgaarden for publicly providing access to a template of a table that can summarize the binary population synthesis settings (<https://github.com/FloorBroekgaarden/templateForTableBPSsettings>). We thank Floor Broekgaarden, Paul D. Lasky, Liang-Duan Liu, Ilya Mandel, Eric Thrane, Xiangyu Ivy Wang, Zepei Xing, and Yun-Wei Yu for helpful discussions. JPZ thanks the COMPAS group at Monash University. YK and LS were supported by the Beijing Natural Science Foundation (1242018), the National SKA Program of China (2020SKA0120300), and the Max Planck Partner Group Program funded by the Max Planck Society. YQ acknowledges the support of Anhui Provincial Natural Science Foundation (grant No. 2308085MA29).

APPENDIX

We summarize the binary population synthesis settings of our COMPAS simulations in Table 4.

REFERENCES

- Abbott, B. P., Abbott, R., Abbott, T. D., et al. 2017a, *PhRvL*, 119, 161101, doi: [10.1103/PhysRevLett.119.161101](https://doi.org/10.1103/PhysRevLett.119.161101)
- . 2017b, *ApJL*, 848, L13, doi: [10.3847/2041-8213/aa920c](https://doi.org/10.3847/2041-8213/aa920c)
- . 2017c, *ApJL*, 848, L12, doi: [10.3847/2041-8213/aa91c9](https://doi.org/10.3847/2041-8213/aa91c9)
- . 2018a, *PhRvL*, 121, 161101, doi: [10.1103/PhysRevLett.121.161101](https://doi.org/10.1103/PhysRevLett.121.161101)
- . 2018b, *Living Reviews in Relativity*, 21, 3, doi: [10.1007/s41114-018-0012-9](https://doi.org/10.1007/s41114-018-0012-9)
- . 2019, *Physical Review X*, 9, 011001, doi: [10.1103/PhysRevX.9.011001](https://doi.org/10.1103/PhysRevX.9.011001)
- Abbott, R., Abbott, T. D., Abraham, S., et al. 2020, *ApJL*, 896, L44, doi: [10.3847/2041-8213/ab960f](https://doi.org/10.3847/2041-8213/ab960f)
- . 2021a, *ApJL*, 915, L5, doi: [10.3847/2041-8213/ac082e](https://doi.org/10.3847/2041-8213/ac082e)
- . 2021b, *Physical Review X*, 11, 021053, doi: [10.1103/PhysRevX.11.021053](https://doi.org/10.1103/PhysRevX.11.021053)
- Abbott, R., Abbott, T. D., Acernese, F., et al. 2023, *Physical Review X*, 13, 041039, doi: [10.1103/PhysRevX.13.041039](https://doi.org/10.1103/PhysRevX.13.041039)
- Abbott, R., Abbott, T. D., Acernese, F., et al. 2023, *Physical Review X*, 13, 011048, doi: [10.1103/PhysRevX.13.011048](https://doi.org/10.1103/PhysRevX.13.011048)
- Acernese, F., Agathos, M., Agatsuma, K., et al. 2015, *Classical and Quantum Gravity*, 32, 024001, doi: [10.1088/0264-9381/32/2/024001](https://doi.org/10.1088/0264-9381/32/2/024001)
- Akmal, A., & Pandharipande, V. R. 1997, *PhRvC*, 56, 2261, doi: [10.1103/PhysRevC.56.2261](https://doi.org/10.1103/PhysRevC.56.2261)
- Alsing, J., Silva, H. O., & Berti, E. 2018, *MNRAS*, 478, 1377, doi: [10.1093/mnras/sty1065](https://doi.org/10.1093/mnras/sty1065)
- Anand, S., Coughlin, M. W., Kasliwal, M. M., et al. 2021, *Nature Astronomy*, 5, 46, doi: [10.1038/s41550-020-1183-3](https://doi.org/10.1038/s41550-020-1183-3)
- Andrews, J. J., Taggart, K., & Foley, R. 2022, *arXiv e-prints*, arXiv:2207.00680, doi: [10.48550/arXiv.2207.00680](https://doi.org/10.48550/arXiv.2207.00680)
- Antoniadis, J., Freire, P. C. C., Wex, N., et al. 2013, *Science*, 340, 448, doi: [10.1126/science.1233232](https://doi.org/10.1126/science.1233232)
- Arcavi, I., Hosseinzadeh, G., Howell, D. A., et al. 2017, *Nature*, 551, 64, doi: [10.1038/nature24291](https://doi.org/10.1038/nature24291)

Table 4. Initial values and default settings of the population synthesis simulation with COMPAS

Description and name	Value/range	Note/setting
Initial conditions		
Initial primary mass $M_{1,i}$	$[5, 150] M_{\odot}$	Kroupa (2001) IMF $\propto M_{1,i}^{-\alpha_{\text{IMF}}}$ with $\alpha_{\text{IMF}} = 2.3$ for stars above $5 M_{\odot}$
Initial mass ratio $q_i = M_{2,i}/M_{1,i}$	$[0, 1]$	We assume a flat mass ratio distribution $p(q_i) \propto 1$ with $M_{2,i} \geq 0.1 M_{\odot}$
Initial semi-major axis a_i	$[0.01, 1000] \text{ AU}$	Distributed flat-in-log $p(a_i) \propto 1/a_i$
Initial metallicity Z_i	$[0.0001, 0.03]$	Distributed using a uniform grid in $\log(Z_i)$ with 10 metallicities
Initial orbital eccentricity e_i	0	All binaries are assumed to be circular at birth
Fiducial parameter settings:		
Stellar winds for hydrogen rich stars	Belczynski et al. (2010a)	Based on Vink & de Koter (2005), including LBV wind mass loss with $f_{\text{LBV}} = 1.5$
Stellar winds for helium stars	Belczynski et al. (2010b)	Based on Hamann & Koesterke (1998) and Vink & de Koter (2005)
Max transfer stability criteria	ζ -prescription	Based on Vigna-Gómez et al. (2018) and references therein
Mass transfer accretion rate	thermal timescale	Limited by thermal timescale for stars Vink & de Koter (2005); Vinciguerra et al. (2020)
Non-conservative mass loss	Eddington-limited	Accretion rate is Eddington-limit for compact objects
	isotropic re-emission	Mashevitch & Yungelson (1975); Bhattacharya & van den Heuvel (1991)
Case BB mass transfer stability	always stable	Soberman et al. (1997); Tauris & van den Heuvel (2006)
CE prescription	$\alpha_{\text{CE}} - \lambda$	Based on Tauris et al. (2015, 2017); Vigna-Gómez et al. (2018)
α_{CE} -parameter	1, 2, 5, 10	Based on Webbink (1984); de Kool (1990)
CE λ -parameter	λ	Based on Xu & Li (2010) and Dominik et al. (2012)
Hertzsprung gap (HG) donor in CE	pessimistic	Defined in Dominik et al. (2012): HG donors don't survive a CE phase
SN natal kick magnitude v_k	$[0, \infty) \text{ km s}^{-1}$	Drawn from Maxwellian distribution with standard deviation σ_{rms}
SN natal kick polar angle θ_k	$[0, \pi]$	$p(\theta_k) = \sin(\theta_k)/2$
SN natal kick azimuthal angle ϕ_k	$[0, 2\pi]$	Uniform $p(\phi) = 1/2\pi$
SN mean anomaly of the orbit	$[0, 2\pi]$	Uniformly distributed
CCSN remnant mass prescription	delayed	From Fryer et al. (2012), which has no lower BH mass gap
USSN remnant mass prescription	delayed	From Fryer et al. (2012)
ECSN remnant mass prescription	$m_f = 1.26 M_{\odot}$	Based on Equation (8) in Timmes et al. (1996)
CCSN velocity dispersion σ_{rms}	100, 265 km s^{-1}	1D rms value based on Hobbs et al. (2005) and Atri et al. (2019)
USSN and ECSN velocity dispersion σ_{rms}	30 km s^{-1}	1D rms value based on e.g., Pfahl et al. (2002); Podsiadlowski et al. (2004)
PISN/PPISN remnant mass prescription	Marchant et al. (2019)	As implemented in Marchant et al. (2019)
Maximum NS mass	$M_{\text{NS,max}} = 2.2 M_{\odot}$	Based on Antoniadis et al. (2013); Alsing et al. (2018); Romani et al. (2022)
Tides and rotation		We do not include prescriptions for tides and/or rotation
Simulation settings		
Total number of binaries sampled per metallicity	10^6	A million binaries per Z_i grid point are simulated
Binary fraction	$f_{\text{bin}} = 1$	
Solar metallicity Z_{\odot}	$Z_{\odot} = 0.0142$	Based on Asplund et al. (2009)
Binary population synthesis code	COMPAS (v02.39.00)	Stevenson et al. (2017); Vigna-Gómez et al. (2018); Neijssel et al. (2019)
		Broekgaarden et al. (2019); Team COMPAS: Riley, J. et al. (2022)

Aso, Y., Michimura, Y., Somiya, K., et al. 2013, PhRvD, 88, 043007, doi: [10.1103/PhysRevD.88.043007](https://doi.org/10.1103/PhysRevD.88.043007)

Asplund, M., Grevesse, N., Sauval, A. J., & Scott, P. 2009, ARA&A, 47, 481, doi: [10.1146/annurev.astro.46.060407.145222](https://doi.org/10.1146/annurev.astro.46.060407.145222)

Atri, P., Miller-Jones, J. C. A., Bahramian, A., et al. 2019, MNRAS, 489, 3116, doi: [10.1093/mnras/stz2335](https://doi.org/10.1093/mnras/stz2335)

Bailyn, C. D., Jain, R. K., Coppi, P., & Orosz, J. A. 1998, ApJ, 499, 367, doi: [10.1086/305614](https://doi.org/10.1086/305614)

Barbieri, C., Salafia, O. S., Perego, A., Colpi, M., & Ghirlanda, G. 2019, A&A, 625, A152, doi: [10.1051/0004-6361/201935443](https://doi.org/10.1051/0004-6361/201935443)

Bardeen, J. M., Press, W. H., & Teukolsky, S. A. 1972, ApJ, 178, 347, doi: [10.1086/151796](https://doi.org/10.1086/151796)

Bavera, S. S., Fragos, T., Qin, Y., et al. 2020, A&A, 635, A97, doi: [10.1051/0004-6361/201936204](https://doi.org/10.1051/0004-6361/201936204)

Belczynski, K., Bulik, T., Fryer, C. L., et al. 2010a, ApJ, 714, 1217, doi: [10.1088/0004-637X/714/2/1217](https://doi.org/10.1088/0004-637X/714/2/1217)

—. 2010b, ApJ, 714, 1217, doi: [10.1088/0004-637X/714/2/1217](https://doi.org/10.1088/0004-637X/714/2/1217)

Belczynski, K., Klencki, J., Fields, C. E., et al. 2020, A&A, 636, A104, doi: [10.1051/0004-6361/201936528](https://doi.org/10.1051/0004-6361/201936528)

Bellm, E. C., Kulkarni, S. R., Graham, M. J., et al. 2019, PASP, 131, 018002, doi: [10.1088/1538-3873/aaecbe](https://doi.org/10.1088/1538-3873/aaecbe)

Bhattacharya, D., & van den Heuvel, E. P. J. 1991, PhR, 203, 1, doi: [10.1016/0370-1573\(91\)90064-S](https://doi.org/10.1016/0370-1573(91)90064-S)

Biscoveanu, S., Landry, P., & Vitale, S. 2023, MNRAS, 518, 5298, doi: [10.1093/mnras/stac3052](https://doi.org/10.1093/mnras/stac3052)

Blandford, R. D., & Znajek, R. L. 1977, MNRAS, 179, 433, doi: [10.1093/mnras/179.3.433](https://doi.org/10.1093/mnras/179.3.433)

Broekgaarden, F. S., Justham, S., de Mink, S. E., et al. 2019, MNRAS, 490, 5228, doi: [10.1093/mnras/stz2558](https://doi.org/10.1093/mnras/stz2558)

Broekgaarden, F. S., Berger, E., Neijssel, C. J., et al. 2021, MNRAS, 508, 5028, doi: [10.1093/mnras/stab2716](https://doi.org/10.1093/mnras/stab2716)

Cao, X.-F., Tan, W.-W., Yu, Y.-W., & Zhang, Z.-D. 2023, arXiv e-prints, arXiv:2306.16795, doi: [10.48550/arXiv.2306.16795](https://doi.org/10.48550/arXiv.2306.16795)

Chandra, K., Gupta, I., Gamba, R., et al. 2024, arXiv e-prints, arXiv:2405.03841, doi: [10.48550/arXiv.2405.03841](https://doi.org/10.48550/arXiv.2405.03841)

- Chattopadhyay, D., Stevenson, S., Broekgaarden, F., Antonini, F., & Belczynski, K. 2022, *MNRAS*, 513, 5780, doi: [10.1093/mnras/stac1283](https://doi.org/10.1093/mnras/stac1283)
- Colombo, A., Duqué, R., Sharan Salafia, O., et al. 2023, arXiv e-prints, arXiv:2310.16894, doi: [10.48550/arXiv.2310.16894](https://doi.org/10.48550/arXiv.2310.16894)
- Coughlin, M., Dietrich, T., Kawaguchi, K., et al. 2017, *ApJ*, 849, 12, doi: [10.3847/1538-4357/aa9114](https://doi.org/10.3847/1538-4357/aa9114)
- Coughlin, M. W., Dietrich, T., Antier, S., et al. 2020, *MNRAS*, 497, 1181, doi: [10.1093/mnras/staa1925](https://doi.org/10.1093/mnras/staa1925)
- Coulter, D. A., Foley, R. J., Kilpatrick, C. D., et al. 2017, *Science*, 358, 1556, doi: [10.1126/science.aap9811](https://doi.org/10.1126/science.aap9811)
- Darbha, S., Kasen, D., Foucart, F., & Price, D. J. 2021, *ApJ*, 915, 69, doi: [10.3847/1538-4357/abff5d](https://doi.org/10.3847/1538-4357/abff5d)
- de Kool, M. 1990, *ApJ*, 358, 189, doi: [10.1086/168974](https://doi.org/10.1086/168974)
- Dominik, M., Belczynski, K., Fryer, C., et al. 2012, *ApJ*, 759, 52, doi: [10.1088/0004-637X/759/1/52](https://doi.org/10.1088/0004-637X/759/1/52)
- D’Orazio, D. J., Haiman, Z., Levin, J., Samsing, J., & Vigna-Gómez, A. 2022, *ApJ*, 927, 56, doi: [10.3847/1538-4357/ac4bdb](https://doi.org/10.3847/1538-4357/ac4bdb)
- Drout, M. R., Piro, A. L., Shappee, B. J., et al. 2017, *Science*, 358, 1570, doi: [10.1126/science.aaq0049](https://doi.org/10.1126/science.aaq0049)
- Drozda, P., Belczynski, K., O’Shaughnessy, R., Bulik, T., & Fryer, C. L. 2022, *A&A*, 667, A126, doi: [10.1051/0004-6361/202039418](https://doi.org/10.1051/0004-6361/202039418)
- Eichler, D., Livio, M., Piran, T., & Schramm, D. N. 1989, *Nature*, 340, 126, doi: [10.1038/340126a0](https://doi.org/10.1038/340126a0)
- Evans, P. A., Cenko, S. B., Kennea, J. A., et al. 2017, *Science*, 358, 1565, doi: [10.1126/science.aap9580](https://doi.org/10.1126/science.aap9580)
- Farr, W. M., Sravan, N., Cantrell, A., et al. 2011, *ApJ*, 741, 103, doi: [10.1088/0004-637X/741/2/103](https://doi.org/10.1088/0004-637X/741/2/103)
- Fernández, R., Kasen, D., Metzger, B. D., & Quataert, E. 2015, *MNRAS*, 446, 750, doi: [10.1093/mnras/stu2112](https://doi.org/10.1093/mnras/stu2112)
- Foucart, F. 2012, *PhRvD*, 86, 124007, doi: [10.1103/PhysRevD.86.124007](https://doi.org/10.1103/PhysRevD.86.124007)
- Foucart, F., Hinderer, T., & Nissanke, S. 2018, *PhRvD*, 98, 081501, doi: [10.1103/PhysRevD.98.081501](https://doi.org/10.1103/PhysRevD.98.081501)
- Fragione, G. 2021, *ApJL*, 923, L2, doi: [10.3847/2041-8213/ac3bcd](https://doi.org/10.3847/2041-8213/ac3bcd)
- Fragione, G., Loeb, A., & Rasio, F. A. 2020, *ApJL*, 895, L15, doi: [10.3847/2041-8213/ab9093](https://doi.org/10.3847/2041-8213/ab9093)
- Fryer, C. L., Belczynski, K., Wiktorowicz, G., et al. 2012, *ApJ*, 749, 91, doi: [10.1088/0004-637X/749/1/91](https://doi.org/10.1088/0004-637X/749/1/91)
- Fuller, J., Piro, A. L., & Jermyn, A. S. 2019, *MNRAS*, 485, 3661, doi: [10.1093/mnras/stz514](https://doi.org/10.1093/mnras/stz514)
- Gao, H., Ai, S.-K., Cao, Z.-J., et al. 2020, *Frontiers of Physics*, 15, 24603, doi: [10.1007/s11467-019-0945-9](https://doi.org/10.1007/s11467-019-0945-9)
- Gehrels, N., Chincarini, G., Giommi, P., et al. 2004, *ApJ*, 611, 1005, doi: [10.1086/422091](https://doi.org/10.1086/422091)
- Goldstein, A., Veres, P., Burns, E., et al. 2017, *ApJL*, 848, L14, doi: [10.3847/2041-8213/aa8f41](https://doi.org/10.3847/2041-8213/aa8f41)
- Gompertz, B. P., Nicholl, M., Smith, J. C., et al. 2023, *MNRAS*, 526, 4585, doi: [10.1093/mnras/stad2990](https://doi.org/10.1093/mnras/stad2990)
- Gompertz, B. P., Cutter, R., Steeghs, D., et al. 2020, *MNRAS*, 497, 726, doi: [10.1093/mnras/staa1845](https://doi.org/10.1093/mnras/staa1845)
- Gottlieb, O., Issa, D., Jacquemin-Ide, J., et al. 2023, *ApJL*, 954, L21, doi: [10.3847/2041-8213/aceeff](https://doi.org/10.3847/2041-8213/aceeff)
- Götz, D., Osborne, J., Cordier, B., et al. 2014, in *Society of Photo-Optical Instrumentation Engineers (SPIE) Conference Series*, Vol. 9144, Space Telescopes and Instrumentation 2014: Ultraviolet to Gamma Ray, ed. T. Takahashi, J.-W. A. den Herder, & M. Bautz, 914423, doi: [10.1117/12.2054898](https://doi.org/10.1117/12.2054898)
- Gupta, A., Gerosa, D., Arun, K. G., et al. 2020, *PhRvD*, 101, 103036, doi: [10.1103/PhysRevD.101.103036](https://doi.org/10.1103/PhysRevD.101.103036)
- Gupta, I., Borhanian, S., Dhani, A., et al. 2023, *PhRvD*, 107, 124007, doi: [10.1103/PhysRevD.107.124007](https://doi.org/10.1103/PhysRevD.107.124007)
- Hamann, W. R., & Koesterke, L. 1998, *A&A*, 335, 1003
- Hayashi, K., Kawaguchi, K., Kiuchi, K., Kyutoku, K., & Shibata, M. 2021, *PhRvD*, 103, 043007, doi: [10.1103/PhysRevD.103.043007](https://doi.org/10.1103/PhysRevD.103.043007)
- Hobbs, G., Lorimer, D. R., Lyne, A. G., & Kramer, M. 2005, *MNRAS*, 360, 974, doi: [10.1111/j.1365-2966.2005.09087.x](https://doi.org/10.1111/j.1365-2966.2005.09087.x)
- Hu, R.-C., Zhu, J.-P., Qin, Y., et al. 2022, *ApJ*, 928, 163, doi: [10.3847/1538-4357/ac573f](https://doi.org/10.3847/1538-4357/ac573f)
- Just, O., Bauswein, A., Ardevol Pulpillo, R., Goriely, S., & Janka, H. T. 2015, *MNRAS*, 448, 541, doi: [10.1093/mnras/stv009](https://doi.org/10.1093/mnras/stv009)
- Kasen, D., Metzger, B., Barnes, J., Quataert, E., & Ramirez-Ruiz, E. 2017, *Nature*, 551, 80, doi: [10.1038/nature24453](https://doi.org/10.1038/nature24453)
- Kasliwal, M. M., Nakar, E., Singer, L. P., et al. 2017, *Science*, 358, 1559, doi: [10.1126/science.aap9455](https://doi.org/10.1126/science.aap9455)
- Kasliwal, M. M., Anand, S., Ahumada, T., et al. 2020, *ApJ*, 905, 145, doi: [10.3847/1538-4357/abc335](https://doi.org/10.3847/1538-4357/abc335)
- Kawaguchi, K., Kyutoku, K., Shibata, M., & Tanaka, M. 2016, *ApJ*, 825, 52, doi: [10.3847/0004-637X/825/1/52](https://doi.org/10.3847/0004-637X/825/1/52)
- Kawaguchi, K., Shibata, M., & Tanaka, M. 2020, *ApJ*, 889, 171, doi: [10.3847/1538-4357/ab61f6](https://doi.org/10.3847/1538-4357/ab61f6)
- Kilpatrick, C. D., Foley, R. J., Kasen, D., et al. 2017, *Science*, 358, 1583, doi: [10.1126/science.aaq0073](https://doi.org/10.1126/science.aaq0073)
- Kroupa, P. 2001, *MNRAS*, 322, 231, doi: [10.1046/j.1365-8711.2001.04022.x](https://doi.org/10.1046/j.1365-8711.2001.04022.x)
- Kyutoku, K., Ioka, K., Okawa, H., Shibata, M., & Taniguchi, K. 2015, *PhRvD*, 92, 044028, doi: [10.1103/PhysRevD.92.044028](https://doi.org/10.1103/PhysRevD.92.044028)
- Kyutoku, K., Ioka, K., & Shibata, M. 2013, *PhRvD*, 88, 041503, doi: [10.1103/PhysRevD.88.041503](https://doi.org/10.1103/PhysRevD.88.041503)

- Langer, N., & Norman, C. A. 2006, *ApJL*, 638, L63, doi: [10.1086/500363](https://doi.org/10.1086/500363)
- Li, L.-X., & Paczyński, B. 1998, *ApJL*, 507, L59, doi: [10.1086/311680](https://doi.org/10.1086/311680)
- LIGO Scientific Collaboration, Aasi, J., Abbott, B. P., et al. 2015, *Classical and Quantum Gravity*, 32, 074001, doi: [10.1088/0264-9381/32/7/074001](https://doi.org/10.1088/0264-9381/32/7/074001)
- LSST Science Collaboration, Abell, P. A., Allison, J., et al. 2009, arXiv e-prints, arXiv:0912.0201, doi: [10.48550/arXiv.0912.0201](https://doi.org/10.48550/arXiv.0912.0201)
- Lyman, J. D., Lamb, G. P., Levan, A. J., et al. 2018, *Nature Astronomy*, 2, 751, doi: [10.1038/s41550-018-0511-3](https://doi.org/10.1038/s41550-018-0511-3)
- Madau, P., & Dickinson, M. 2014, *ARA&A*, 52, 415, doi: [10.1146/annurev-astro-081811-125615](https://doi.org/10.1146/annurev-astro-081811-125615)
- Mandel, I., & Müller, B. 2020, *MNRAS*, 499, 3214, doi: [10.1093/mnras/staa3043](https://doi.org/10.1093/mnras/staa3043)
- Mandel, I., & Smith, R. J. E. 2021, *ApJL*, 922, L14, doi: [10.3847/2041-8213/ac35dd](https://doi.org/10.3847/2041-8213/ac35dd)
- Marchant, P., Renzo, M., Farmer, R., et al. 2019, *ApJ*, 882, 36, doi: [10.3847/1538-4357/ab3426](https://doi.org/10.3847/1538-4357/ab3426)
- Massevitch, A., & Yungelson, L. 1975, *Mem. Soc. Astron. Italiana*, 46, 217
- Metzger, B. D., Martínez-Pinedo, G., Darbha, S., et al. 2010, *MNRAS*, 406, 2650, doi: [10.1111/j.1365-2966.2010.16864.x](https://doi.org/10.1111/j.1365-2966.2010.16864.x)
- Narayan, R., Paczynski, B., & Piran, T. 1992, *ApJL*, 395, L83, doi: [10.1086/186493](https://doi.org/10.1086/186493)
- Neijssel, C. J., Vigna-Gómez, A., Stevenson, S., et al. 2019, *MNRAS*, 490, 3740, doi: [10.1093/mnras/stz2840](https://doi.org/10.1093/mnras/stz2840)
- Özel, F., Psaltis, D., Narayan, R., & McClintock, J. E. 2010, *ApJ*, 725, 1918, doi: [10.1088/0004-637X/725/2/1918](https://doi.org/10.1088/0004-637X/725/2/1918)
- Paczynski, B. 1986, *ApJL*, 308, L43, doi: [10.1086/184740](https://doi.org/10.1086/184740)
- . 1991, *AcA*, 41, 257
- Pannarale, F. 2013, *PhRvD*, 88, 104025, doi: [10.1103/PhysRevD.88.104025](https://doi.org/10.1103/PhysRevD.88.104025)
- Panther, B., Heavens, A. F., & Jimenez, R. 2004, *MNRAS*, 355, 764, doi: [10.1111/j.1365-2966.2004.08355.x](https://doi.org/10.1111/j.1365-2966.2004.08355.x)
- Pfahl, E., Rappaport, S., & Podsiadlowski, P. 2002, *ApJ*, 573, 283, doi: [10.1086/340494](https://doi.org/10.1086/340494)
- Pian, E., D’Avanzo, P., Benetti, S., et al. 2017, *Nature*, 551, 67, doi: [10.1038/nature24298](https://doi.org/10.1038/nature24298)
- Podsiadlowski, P., Langer, N., Poelarends, A. J. T., et al. 2004, *ApJ*, 612, 1044, doi: [10.1086/421713](https://doi.org/10.1086/421713)
- Qin, Y., Fragos, T., Meynet, G., et al. 2018, *A&A*, 616, A28, doi: [10.1051/0004-6361/201832839](https://doi.org/10.1051/0004-6361/201832839)
- Rivinius, T., Baade, D., Hadrava, P., Heida, M., & Klement, R. 2020, *A&A*, 637, L3, doi: [10.1051/0004-6361/202038020](https://doi.org/10.1051/0004-6361/202038020)
- Romani, R. W., Kandel, D., Filippenko, A. V., Brink, T. G., & Zheng, W. 2022, *ApJL*, 934, L17, doi: [10.3847/2041-8213/ac8007](https://doi.org/10.3847/2041-8213/ac8007)
- Ronchini, S., Bala, S., Wood, J., et al. 2024, arXiv e-prints, arXiv:2405.10752. <https://arxiv.org/abs/2405.10752>
- Salafia, O. S., Ghisellini, G., Pescalli, A., Ghirlanda, G., & Nappo, F. 2015, *MNRAS*, 450, 3549, doi: [10.1093/mnras/stv766](https://doi.org/10.1093/mnras/stv766)
- Sarin, N., Lasky, P. D., Vivanco, F. H., et al. 2022, *PhRvD*, 105, 083004, doi: [10.1103/PhysRevD.105.083004](https://doi.org/10.1103/PhysRevD.105.083004)
- Savchenko, V., Ferrigno, C., Kuulkers, E., et al. 2017, *ApJL*, 848, L15, doi: [10.3847/2041-8213/aa8f94](https://doi.org/10.3847/2041-8213/aa8f94)
- Shao, Y., & Li, X.-D. 2021, *ApJ*, 920, 81, doi: [10.3847/1538-4357/ac173e](https://doi.org/10.3847/1538-4357/ac173e)
- Shibata, M., & Taniguchi, K. 2011, *Living Reviews in Relativity*, 14, 6, doi: [10.12942/lrr-2011-6](https://doi.org/10.12942/lrr-2011-6)
- Siegel, D. M., & Metzger, B. D. 2017, *PhRvL*, 119, 231102, doi: [10.1103/PhysRevLett.119.231102](https://doi.org/10.1103/PhysRevLett.119.231102)
- Smartt, S. J., Chen, T. W., Jerkstrand, A., et al. 2017, *Nature*, 551, 75, doi: [10.1038/nature24303](https://doi.org/10.1038/nature24303)
- Soberman, G. E., Phinney, E. S., & van den Heuvel, E. P. J. 1997, *A&A*, 327, 620
- Song, H.-R., Ai, S.-K., Wang, M.-H., et al. 2019, *ApJL*, 881, L40, doi: [10.3847/2041-8213/ab3921](https://doi.org/10.3847/2041-8213/ab3921)
- Stevenson, S., Vigna-Gómez, A., Mandel, I., et al. 2017, *Nature Communications*, 8, 14906, doi: [10.1038/ncomms14906](https://doi.org/10.1038/ncomms14906)
- Tagawa, H., Kocsis, B., Haiman, Z., et al. 2021, *ApJ*, 908, 194, doi: [10.3847/1538-4357/abd555](https://doi.org/10.3847/1538-4357/abd555)
- Tanaka, M., Kato, D., Gaigalas, G., & Kawaguchi, K. 2020, *MNRAS*, 496, 1369, doi: [10.1093/mnras/staa1576](https://doi.org/10.1093/mnras/staa1576)
- Tauris, T. M., Langer, N., & Podsiadlowski, P. 2015, *MNRAS*, 451, 2123, doi: [10.1093/mnras/stv990](https://doi.org/10.1093/mnras/stv990)
- Tauris, T. M., & van den Heuvel, E. P. J. 2006, *Formation and evolution of compact stellar X-ray sources*, Vol. 39, 623–665
- Tauris, T. M., Kramer, M., Freire, P. C. C., et al. 2017, *ApJ*, 846, 170, doi: [10.3847/1538-4357/aa7e89](https://doi.org/10.3847/1538-4357/aa7e89)
- Team COMPAS: Riley, J., Agrawal, P., Barrett, J. W., et al. 2022, *ApJS*, 258, 34, doi: [10.3847/1538-4365/ac416c](https://doi.org/10.3847/1538-4365/ac416c)
- The LIGO Scientific Collaboration, the Virgo Collaboration, & the KAGRA Collaboration. 2024, arXiv e-prints, arXiv:2404.04248. <https://arxiv.org/abs/2404.04248>
- The LIGO Scientific Collaboration, the Virgo Collaboration, Abbott, R., et al. 2021, arXiv e-prints, arXiv:2108.01045, doi: [10.48550/arXiv.2108.01045](https://doi.org/10.48550/arXiv.2108.01045)
- Thompson, T. A., Kochanek, C. S., Stanek, K. Z., et al. 2019, *Science*, 366, 637, doi: [10.1126/science.aau4005](https://doi.org/10.1126/science.aau4005)

- Timmes, F. X., Woosley, S. E., & Weaver, T. A. 1996, *ApJ*, 457, 834, doi: [10.1086/176778](https://doi.org/10.1086/176778)
- Troja, E., van Eerten, H., Zhang, B., et al. 2020, *MNRAS*, 498, 5643, doi: [10.1093/mnras/staa2626](https://doi.org/10.1093/mnras/staa2626)
- Typel, S., Röpke, G., Klähn, T., Blaschke, D., & Wolter, H. H. 2010, *PhRvC*, 81, 015803, doi: [10.1103/PhysRevC.81.015803](https://doi.org/10.1103/PhysRevC.81.015803)
- Vigna-Gómez, A., Neijssel, C. J., Stevenson, S., et al. 2018, *MNRAS*, 481, 4009, doi: [10.1093/mnras/sty2463](https://doi.org/10.1093/mnras/sty2463)
- Vinciguerra, S., Neijssel, C. J., Vigna-Gómez, A., et al. 2020, *MNRAS*, 498, 4705, doi: [10.1093/mnras/staa2177](https://doi.org/10.1093/mnras/staa2177)
- Vink, J. S., & de Koter, A. 2005, *A&A*, 442, 587, doi: [10.1051/0004-6361:20052862](https://doi.org/10.1051/0004-6361:20052862)
- Wang, T., Liu, G., Cai, Z., et al. 2023, *Science China Physics, Mechanics, and Astronomy*, 66, 109512, doi: [10.1007/s11433-023-2197-5](https://doi.org/10.1007/s11433-023-2197-5)
- Wang, Z.-H.-T., Hu, R.-C., Qin, Y., et al. 2024, *arXiv e-prints*, arXiv:2401.17558, doi: [10.48550/arXiv.2401.17558](https://doi.org/10.48550/arXiv.2401.17558)
- Webbink, R. F. 1984, *ApJ*, 277, 355, doi: [10.1086/161701](https://doi.org/10.1086/161701)
- Wyrzykowski, L., & Mandel, I. 2020, *A&A*, 636, A20, doi: [10.1051/0004-6361/201935842](https://doi.org/10.1051/0004-6361/201935842)
- Xing, Z., Bavera, S. S., Fragos, T., et al. 2024, *A&A*, 683, A144, doi: [10.1051/0004-6361/202347971](https://doi.org/10.1051/0004-6361/202347971)
- Xu, X.-J., & Li, X.-D. 2010, *ApJ*, 716, 114, doi: [10.1088/0004-637X/716/1/114](https://doi.org/10.1088/0004-637X/716/1/114)
- Ye, C., & Fishbach, M. 2022, *ApJ*, 937, 73, doi: [10.3847/1538-4357/ac7f99](https://doi.org/10.3847/1538-4357/ac7f99)
- Ye, C. S., Fong, W.-f., Kremer, K., et al. 2020, *ApJL*, 888, L10, doi: [10.3847/2041-8213/ab5dc5](https://doi.org/10.3847/2041-8213/ab5dc5)
- Zhang, B. 2018, *The Physics of Gamma-Ray Bursts* (Cambridge University Press), doi: [10.1017/9781139226530](https://doi.org/10.1017/9781139226530)
- Zhang, B., & Mészáros, P. 2002, *ApJ*, 571, 876, doi: [10.1086/339981](https://doi.org/10.1086/339981)
- Zhang, B. B., Zhang, B., Sun, H., et al. 2018, *Nature Communications*, 9, 447, doi: [10.1038/s41467-018-02847-3](https://doi.org/10.1038/s41467-018-02847-3)
- Zhu, J.-P., Qin, Y., Wang, Z.-H.-T., et al. 2024, *MNRAS*, 529, 4554, doi: [10.1093/mnras/stae815](https://doi.org/10.1093/mnras/stae815)
- Zhu, J.-P., Wang, X. I., Sun, H., et al. 2022a, *ApJL*, 936, L10, doi: [10.3847/2041-8213/ac85ad](https://doi.org/10.3847/2041-8213/ac85ad)
- Zhu, J.-P., Wu, S., Qin, Y., et al. 2022b, *ApJ*, 928, 167, doi: [10.3847/1538-4357/ac540c](https://doi.org/10.3847/1538-4357/ac540c)
- Zhu, J.-P., Wu, S., Yang, Y.-P., et al. 2021a, *ApJ*, 921, 156, doi: [10.3847/1538-4357/ac19a7](https://doi.org/10.3847/1538-4357/ac19a7)
- Zhu, J.-P., Yang, Y.-P., Liu, L.-D., et al. 2020, *ApJ*, 897, 20, doi: [10.3847/1538-4357/ab93bf](https://doi.org/10.3847/1538-4357/ab93bf)
- Zhu, J.-P., Wu, S., Yang, Y.-P., et al. 2021b, *ApJ*, 917, 24, doi: [10.3847/1538-4357/abfe5e](https://doi.org/10.3847/1538-4357/abfe5e)
- . 2023, *ApJ*, 942, 88, doi: [10.3847/1538-4357/aca527](https://doi.org/10.3847/1538-4357/aca527)